E.M. Godzhayev, J.I. Guseinov

E.M. Godzhayev

[1]Azerbaijan Technical University, 25, Huseyn Javid Ave., Baku, AZ1073, Republic Azerbaijan
[2]Azerbaijan State Pedagogical University, Uzeir Hajibeyov Str., 34, Baku, Azerbaijan

PHYSICO-CHEMICAL ANALYSIS AND THERMOELECTRIC PROPERTIES OF $(SnSe)_{1-x}(ErSe)_x$ SYSTEM ALLOYS

J.I. Guseinov

In this paper, a diagram of state of SnSe-ErSe system has been constructed, and SnSe based solubility in this system has been established. Atomic-force microscope has been used to study surface microrelief of SnSe single crystal, X-ray phase analysis has been performed and the temperature dependences of the electric conductivity, the Hall coefficient, the Seebeck coefficient and the thermal conductivity of $(SnSe)_{1-x}(ErSe)_x$ *system alloys have been investigated.*

Key words: $(SnSe)_{1-x}(ErSe)_x$ system, atomic-force microscope, thermoelectric figure of merit, X-ray phase analysis.

Introduction

Chalcogenides of *SnX* type hold a special place among semiconductor compounds. These compounds possess switching properties, are high pressure sensors and valuable thermoelectric materials [1-3].

Selenium and tin solid solutions also possess high thermoelectric figure of merit and photosensitivity [3-5]. Information is found in the literature on the research of *Sn-Ln-X* (*Ln* = *La* – *Lu*; *X* = *S*, *Se*, *Te*) systems, where it is revealed that substitution solid solutions are formed in these systems close to *SnX* [6, 7]. In particular, physicochemical and X-ray phase analyses in the concentration range of 0 – 10 *ErSe* have established that in this system the solubility of *ErSe* in *SnSe* at 600 °C makes 6.3 mol. %, and at 900 °C - 5 mol. %. However, phase analysis in a wider concentration range and investigation of alloy properties has not been performed. In this connection, the purpose of this paper is physicochemical analysis, study of surface microrelief, research on the thermoelectric properties of *SnSe* – *ErSe* system alloys.

Experimental

In the synthesis of ternary alloys of *SnSe-ErSe* system, special purity elements were employed as the source components, namely “B4-000” tin, “OC417-4” selenium and chemically pure elemental erbium “ER-2”.

To construct a diagram of state, alloys were prepared that comprised components in different ratios (with the interval 5 mol.%) of weight 2 g.

Calcined aluminium oxide was used as a reference for differential recording. The rate of samples heating and cooling was 0.5 K/s. The temperatures in the construction of the diagram of state were determined to an accuracy of 2 – 2.5 K.

The alloys of *SnSe-ErSe* system were synthesized of the source components in evacuated to 0.1333 Pa quartz ampoules. Synthesis took place in two steps: at first the ampoules with the substance were heated at a rate of 4 – 5 degrees/min to selenium melting point and held at this temperature for 3 – 4 hours, following which the temperature was increased to 950 – 1000 °C depending on the composition and held for 8 – 9 hours. Homogenizing annealing of the resulting samples was performed at 580 °C for 120 hours.

Synthesized samples for differential thermal analysis and electrophysical investigations were subject to homogenizing annealing for 100 – 110 hours depending on the composition, namely annealing was increased with increasing erbium content.

Differential thermal analysis of the samples was done on a low-frequency thermal recorder NTR- 73 with a chromel-alumel thermocouple. Heating rate was 8 degrees/min.

X-ray phase analysis was done on a diffractometer DRON-3 with CuK_α-radiation and nickel filter.

The microhardness of alloys was determined by metallographic method on PMT-3 under the loads selected as a result of studying microhardness measurement for each phase as a function of load. The density of alloys was determined by picnometer and X-ray methods, with toluene used as filler.

Discussion of the results

The resulting alloys are compact, with metallic lustre, and with increasing erbium content their colour becomes dark grey and changes to black. The alloys are resistant to air and water. They are decomposed by concentrated mineral acids (*HCl*, HNO_3, H_2SO_4) and alcali (*NaOH*, *KOH*), whereas organic solvents have no effect on them.

The results of differential thermal analysis of *SnSe-ErSe* system alloys have shown that all fixed effects on heating and cooling curves are reversible.

As a result of microstructure study, a restricted solubility area was detected close to *SnSe.* To confirm the area boundary of solid solutions based on *SnSe*, extra alloys comprising 3, 4, 5 and 6 mol.% *ErSe* were synthesized. The alloys were annealed at 760 °C for 160 hours, and then hardened.

According to the results of microstructural analysis, the solubility of *ErSe* in *SnSe* at room temperature is 5 mol.%, and at temperature close to eutectic point it comes to 10 mol.%. In the range of 5 – 40 mol.% of *ErSe* all the alloys are two-phase. X-ray phase analysis of the alloys (Table 1) has shown that on the diffractograms in the concentration range of 0 – 5 mol.% *ErSe* the diffraction maxima are identical.

With increasing erbium content in *SnSe*, on the diffractograms of alloys there appear new, uncharacteristic of *SnSe,* maxima that are related to *ErSe*.

Table 2 gives some data of physicochemical analysis. As can be seen from the table, in the alloys from solid-solution range, with increase in erbium concentration, the microhardness is increased (480 – 620MPa). The density of alloys from solid-solution range is monotonously increased.

Based on the results of integrated physicochemical analyses, a microdiagram of *SnSe-ErSe* system was constructed (Fig. 1) As it follows from Fig. 1, the system liquidus consists of two parts. In the concentration range of 0 – 10 mol.% *ErSe,* α-phase is primarily crystallized from the liquid (*SnSe* based solid solutions). Then *ErSe* phase is crystallized from the liquid. Two-phase alloys (α + *ErSe*) are crystallized below the liquidus line.

Table 1

Results of X-ray phase analysis of $Sn_{1-x}Er_xSe$ alloys

Hkl	Θ	d_{theor}, Å	d_{exp}, Å	I/I_0	Θ	d_{theor}, Å	d_{exp}, Å	I/I_0	Θ	d_{theor}, Å	d_{exp}, Å	I/I_0	Θ	d_{theor}, Å	d_{exp}, Å	I/I_0	Θ	d_{theor}, Å	d_{exp}, Å	I/I_0
	SnSe $a = 4.46$; $b = 4.19$; $c = 11.57$ Å				$Sn_{0.99}Er_{0.01}Se$ $a = 4.468$; $b = 4.206$; $c = 11.59$ Å				$Sn_{0.98}Er_{0.02}Se$ $a = 4.471$; $b = 4.221$; $c = 11.60$ Å				$Sn_{0.97}Er_{0.03}Se$ $a = 4.477$; $b = 4.229$; $c = 11.61$ Å				$Sn_{0.96}Er_{0.04}Se$ $a = 4.481$; $b = 4.236$; $c = 11.62$ Å			
1	2	3	4	5	6	7	8	9	10	11	12	13	14	15	16	17	18	19	20	21
101	$10^042`$	4.1615	4.1605	10	$10^041`$	4.1691	4.1604	9	$10^039`$	4.1718	4.1724	8	$10^039`$	4.1775	4.1782	7	$10^037`$	4.1810	4.1822	5
102	$12^036`$	3.5321	3.5316	68	$12^035`$	3.5388	3.5391	59	$12^034`$	3.5411	3.5432	56	$10^039`$	3.5458	3.5466	53	$12^033`$	3.5487	3.5496	49
110	$14^012`$	3.0537	3.0534	3	$14^035`$	3.0625	3.0611	3	$14^032`$	3.0692	3.0704	3	$10^039`$	3.0743	3.0749	3	$14^030`$	3.0782	3.0794	3
111	$15^008`$	2.9526	2.9523	16	$15^03`$	2.9609	2.9700	11	$15^03`$	2.9671	2.9402	9	$10^039`$	2.9717	2.9727	7	$15^001`$	2.9757	2.9763	5
004	$15^027`$	2.8925	2.8924	100	$15^026`$	2.8985	2.8974	93	$15^024`$	2.9002	2.9016	90	$10^039`$	2.904	2.9016	87	$15^023`$	2.9060	2.9069	85
113	$18^047`$	2.3941	2.3939	11	$18^043`$	2.4002	2.4032	8	$18^042`$	2.4040	2.4048	6	$10^039`$	2.4077	2.4085	5	$18^038`$	2.4102	2.4114	4
201	$20^037`$	2.1897	2.1907	2	$20^034`$	2.1936	2.1944	2	$20^033`$	2.1951	2.1960	2	$10^039`$	2.1980	2.1988	2	$20^029`$	2.2000	2.2041	2
202	$21^045`$	2.0807	2.0814	5	$21^041`$	2.0845	2.0863	3	$21^041`$	2.0859	2.0866	3	$10^039`$	2.0887	2.0896	3	$21^038`$	2.0905	2.0912	2
105	$21^058`$	2.054	2.0611	2	$21^059`$	2.0581	2.0592	2	$21^059`$	2.0594	2.0591	2	$10^039`$	2.0620	2.0634	2	$21^056`$	2.0636	2.0642	2
006	$23^034`$	1.9283	1.9280	4	$23^032`$	1.9323	1.9909	3	$23^029`$	1.9335	1.9346	3	$10^039`$	1.9360	1.9371	3	$23^026`$	1.9373	1.9382	2
115	$24^043`$	1.8443	1.8435	14	$24^039`$	1.8486	1.8481	12	$24^036`$	1.8508	1.8514	10	$10^039`$	1.8535	1.8549	8	$24^033`$	1.8551	1.8559	6
204	$25^058`$	1.7660	1.7609	2	$25^049`$	1.7694	1.7704	2	$25^048`$	1.7705	1.7712	2	$10^039`$	1.7729	1.7738	2	$25^044`$	1.7743	1.7751	2
213	$26^08`$	1.7533	1.7516	5	$26^02`$	1.7572	1.7563	3	$25^059`$	1.7592	1.7599	3	$10^039`$	1.7617	1.7624	3	$25^054`$	1.7635	1.7649	3
205	$28^037`$	1.6057	1.6094	3	$28^043`$	1.6088	1.6043	2	$28^036`$	1.6098	1.6104	2	$10^039`$	1.6120	1.6194	2	$28^025`$	1.6132	1.6134	2
008	$32^012`$	1.4462	1.4462	39	$32^07`$	1.4492	1.4499	36	$32^04`$	1.4501	1.4518	34	$10^039`$	1.4520	1.4529	31	$32^03`$	1.4531	1.4542	27

Table 2

Results of differential thermal and X-ray phase analysis of the density and micro hardness of SnSe-ErSe system alloys

№	Molecular composition, %		Unit cell volume, V, Å^3	Density, 10^3kg/m^3		Phase micro hardness, MPa	Unit cell parameters, Å		
	SnSe	*ErSe*		ρ_{peak}	$\rho_{X\text{-}ray}$		*a*	*b*	*c*
1	100	0	216.21	6.18	6.28	480	4.460	4.190	11.570
2	99	1	217.88	6.20	6.38	520	4.468	4.206	11.594
3	98	2	218.93	6.20	6.40	540	4.471	4.221	11.601
4	97	3	219.93	6.21	6.42	570	4.477	4.229	11.616
5	96	4	220.64	6.23	6.42	620	4.481	4.236	11.624

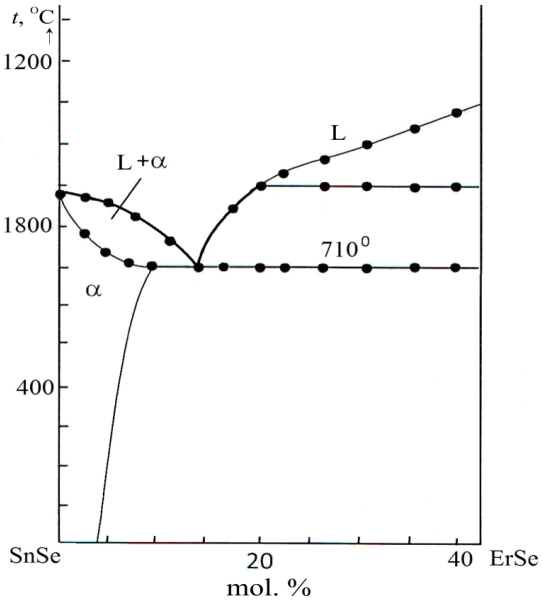

Fig. 1. Diagram of state of SnSe-ErSe system.

We have investigated the surface relief of *SnSe* single crystal using scanning probe microscope method in atomic-force mode (AFM) [8].

As a result, we obtained plane surface images of *SnSe* single crystal of size $5{\cdot}10^3 \times 5{\cdot}10^3$ nm (Fig. 2, *b*). The AFM image resulted from increasing the most homogeneous surface part. From Fig. 2, *a* showing 3-D images of the same parts it is seen that surface relief of a single crystal is uniform enough. The analysis of AFM image histogram (Fig. 2, *c*) shows that surface uniformity varies within 25 nm. It is obvious that though *SnSe* belongs to layered semiconductors with a natural surface cleavage, in the near-boundary layer there is still some roughness which is most likely due to the fact that at destruction of bonding forces not individual atoms, but their groups – clusters, remain on crystal surface.

This is also proved by the Fourier spectrum obtained by the AFM method (Fig. 2, *d*). Concentration of spectrum in the image centre shows that surface particles have about identical dimensions, i.e. they are commensurable.

The paper investigated the temperature dependences of the electric conductivity, the Hall coefficient, the thermoelectric figure of merit in the temperature range of 77 – 900 K, and the thermal conductivity in the temperature range of 77 – 350 °K of $Sn_{1-x}Er_xSe$ alloys. The results of investigation are given in Fig. 3. As it follows from Fig. 3 *a*, a change in the electric conductivity of the source compound *SnSe* and $Sn_{1-x}Er_xSe$ solid solutions on its basis with temperature are similar, i.e. at low temperatures there is a relatively weak electric conductivity increase at the cost of electrons

that passed from impurity levels to conduction band. At room temperature the number of carriers that passed from impurity levels to conduction band is stabilized and, hence, the electric conductivity is reduced due to a reduction of the Hall mobility, and with the onset of intrinsic conductivity it is increased due to increase in the concentration of intrinsic carriers.

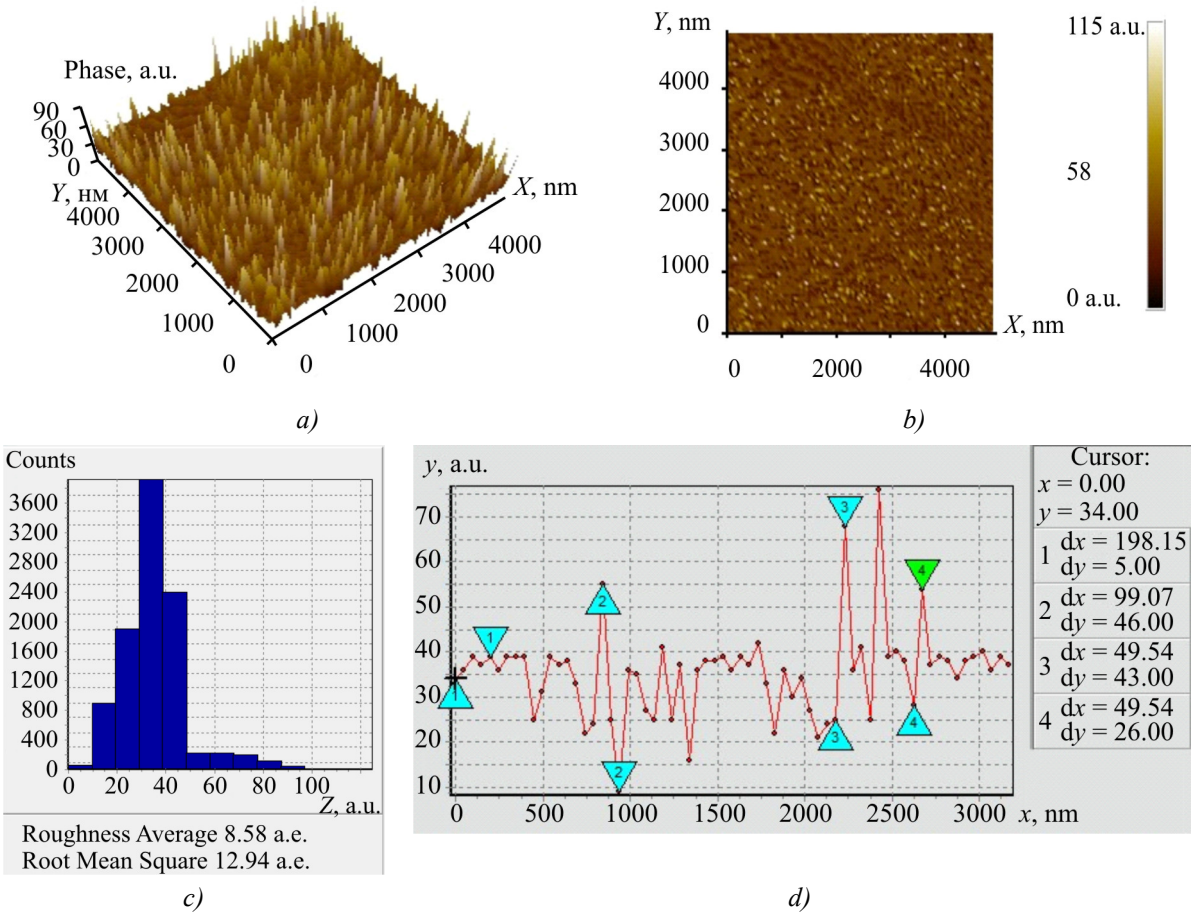

Fig. 2. (a) – 3D, (b) – two-dimensional AFM image of surface, (c) – surface histogram, (d) –Fourier spectrum of SnSe single crystal of size 5 μm.

A change in the Hall coefficient with temperature agrees well with the temperature change of the electric conductivity of $Sn_{1-x}Er_xSe$ crystals (Fig. 3, *b*), i.e. at low temperatures *R* remains constant, and with the onset of intrinsic conductivity it is reduced with a rise in temperature. The Seebeck coefficient of crystals at low temperatures in the field of impurity conductivity is increased, and with the onset of intrinsic conductivity it is reduced (Fig. 3, *c*), which is typical of semiconductor compounds and solid solutions with a complex band structure. The energy gap width of $Sn_{1-x}Er_xSe$ crystals was determined to an accuracy of 0.004 eV. The values of energy gap width calculated from the temperature dependences of the electric conductivity and the Hall coefficient correlate well. This testifies to the fact that all investigated samples are characterized by one predominant impurity level.

It is established that with a substitution of erbium atoms for tin atoms in *SnSe* lattice the energy gap width is reduced, i.e. for *SnSe* it was 0.86 eV, and for $Sn_{0.075}Er_{0.025}Se$ and $Sn_{0.095}Er_{0.05}Se$ compositions - 0.83 and 0.81 eV, respectively.

The thermal conductivity of solid $Sn_{1-x}Er_xSe$ was measured by a steady-state method. Investigations were pursued in the temperature range of 80 – 330 K. The results of research are given

in Fig. 3, *d*. As it follows from Fig. 3, *d*, the thermal conductivity of *SnSe* with a variation of cation composition along the direction of increasing atomic weights of substitution cations is regularly decreased. However, when passing from *SnSe* with the ordered arrangement of atoms to substitution solid solutions on its basis, there are deviations from a regular change in the thermal conductivity as a function of atomic weight. Apparently, this is due to the fact that for $Sn_{1-x}Er_xSe$ crystals prevalent is phonon scattering from local point defects, and the main factor that affects thermal resistance is local density variation and change in elastic properties of the medium. Local density variation mainly depends on the difference in average atomic weights, and local changes in elastic properties – on the difference in atomic radii of the solvent and dissolved material.

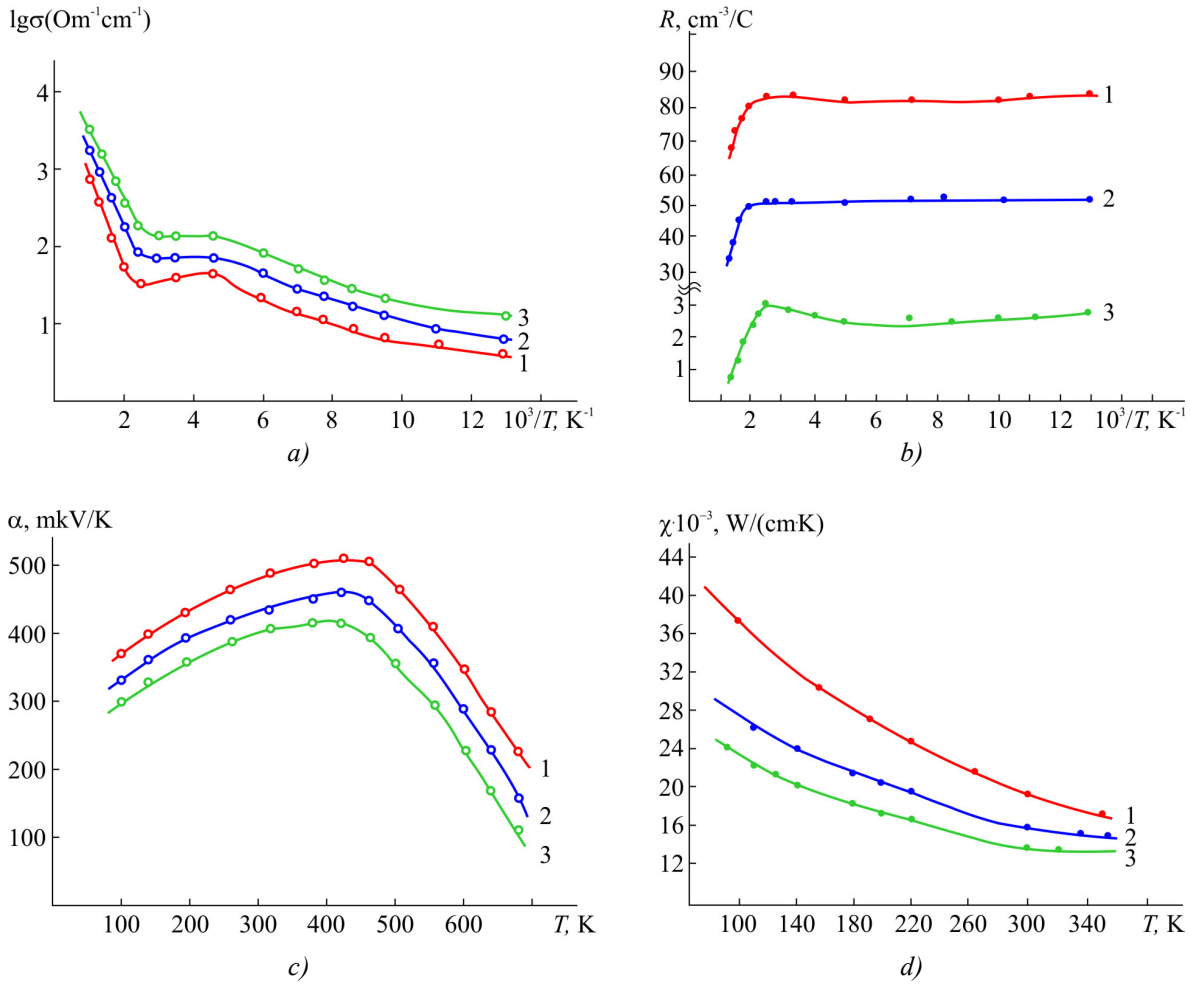

Fig. 3. Temperature dependences of the electric conductivity (a), the Hall coefficient (b), the Seebeck coefficient (c) and the thermal conductivity of $Sn_{1-x}Er_xSe$ crystals where 1 – x = 0; 2 – x = 0.02; 3 – x = 0.04.

Our experimental results suggest that with increasing erbium content in $Sn_{1-x}Er_xSe$ solid solutions, their electric conductivity is increased and thermal conductivity is decreased. Therefore, one would expect that in this system in certain compositions and in certain temperature range the thermoelectric figure of merit will reach the value which is of practical significance. The results of calculation are given in Table 3. As it follows from the table, for $Sn_{0.96}Er_{0.04}Se$ composition in the temperature range of 250 – 300 K the thermoelectric figure of merit proves to be high $(1.36 – 1.81)\cdot10^{-3}$ K^{-1} and is of practical interest.

Table 3

Thermoelectric parameters of $Sn_{1-x}Er_xSe$ alloys

T, K	*SnSe*				$Sn_{0.98}Er_{0.02}Se$				$Sn_{0.96}Er_{0.04}Se$			
	σ_1, $Ohm^{-1}\cdot cm^{-1}$	α_1, μV/K	χ_1, W /(cm·K)	$Z_1\cdot10^3$, K^{-1}	σ_2, $Ohm^{-1}\cdot cm^{-1}$	α_2, μV/K	χ_2, W/(cm·K)	$Z_2\cdot10^3$, K^{-1}	σ_3, $Ohm^{-1}\cdot cm^{-1}$	α_3, μV/K	χ_3, W/(cm·K)	$Z_3\cdot10^3$, K^{-1}
100	56.23	370	37	0.21	11.2	330	27.5	0.44	17.8	300	23.2	0.69
125	10	390	34.6	0.44	22.4	350	25.4	0.11	35.5	320	21.2	0.17
167	20	403	29.4	0.11	44.7	375	22.4	0.28	79.4	335	19	0.47
250	44.67	460	22.2	0.43	79	420	17.6	0.79	141.3	380	15	1.36
300	31.6	480	19.6	0.37	63.1	435	15.8	0.76	158.5	400	14	1.81

Conclusion

Physicochemical analysis methods have been used to construct the diagram of state of *SnSe*-40 mol.% *ErSe* section, and it has been established that in this system *SnSe* based solid solutions are formed in the region of ($0 \le x \le 0.04$). Surface microrelief and the temperature dependences of the electric conductivity, the Hall coefficient, the Seebeck coefficient, and the thermal conductivity have been investigated and the thermoelectric figure of merit of $Sn_{1-x}Er_xSe$ alloys has been calculated.

References

1. N.Kh.Abrikosov, V.F.Bankina, A.V.Poretskaya, and E.D.Skudnogo, *Semiconductor Compounds, their Preparation and Properties* (Moscow: Nauka, 1967), 220 p.
2. *P.S.Yerofeev, O.V.Salamatnikova, V.S.Gaidukova, and S.I.Repenko,* On the Issue of Interaction between Monochalcogenides of Bivalent IV Group Elements and Rare-Earth Metals, *Chalcogenides, Issue 3* (Kyiv: Naukova Dumka, 1974), p.87.
3. *N.Kh.Abrikosov, L.E.Shelimova, Semiconductor Materials Based on $A^{IV}B^{VI}$ Compounds* (Moscow: Nauka, 1975), 195 p.
4. *N.Bouad, M.-C.Record, J.-C.Tedenac, and R.-M.Marin-Ayral,* Mechanical Alloying of a Thermoelectric Alloy: $Pb_{0.65}Sn_{0.35}Te$, *J. Solid State Chem*. **177** (1), 221-226 (2004).
5. *A.E.Klimov, V.N.Shumskiy, Photosensitivity of $Pb_{1-x}Sn_xTe$ <İn> Films in the Intrinsic Absorption Range, Semiconductors* **42**(2), 147-152 (2008)
6. *A.P.Gurshumov, B.B.Kuliev, A.M.Akhmedov,* Diagrams of State of Metal Systems, Ed. by L.A.Petrova (Moscow, 1986, issue 29), p.429-430.
7. A.P.Gurshumov, B.B.Kuliev, A.M.Akhmedov, D.M.Safarov, and V.B.Lazarev, Interaction between Tin Monoselenide and Monoselenides of Rare-Earth Materials, *Izvestiya AN SSSR, Inorganic Materials* **20** (7), 1090-1093 (1984).
8. *V.Mironov, Fundamentals of Scanning Probe Microscopy* (Moscow: Technosphera, 2004), p. 197-201.

Submitted.25.02.14